THE JOURNAL OF PHYSICAL CHEMISTRY C

pubs.acs.org/JPCC Article

Identification of the Active Sites in the Dehydrogenation of Methanol on Pt/Al_2O_3 Catalysts

Tianjun Xie, Bryan J. Hare, Paul J. Meza-Morales, Carsten Sievers, and Rachel B. Getman*

Cite This: J. Phys. Chem. C 2020, 124, 19015−19023 Read Online

ACCESS | Metrics & More | Article Recommendations | Supporting Information

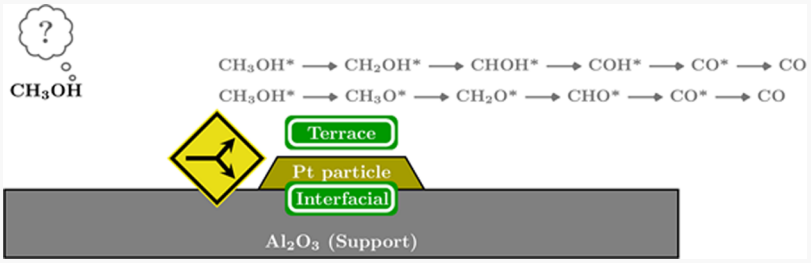

ABSTRACT: Conversion of oxygenates derived from biomass is a promising strategy for the production of fuels and chemicals. The needed H_2 can be supplied simultaneously (and sustainably) via aqueous phase reforming (APR; $C_nH_{2n}O_n + nH_2O \rightarrow nCO_2 + 2nH_2$). APR is typically carried out over supported metal catalysts under liquid water. Dehydrogenation is the first constituent reaction in APR and involves both C−H and O−H bond cleavages; however, details about the mechanism and natures of the active sites remain unknown. Herein, such details are provided for methanol dehydrogenation over a supported Pt/Al_2O_3 catalyst. Using density functional theory calculations, we find that methanol dehydrogenation occurs on the Pt terraces and at the Pt/Al_2O_3 interfaces but follows different paths: on interfacial sites, O−H cleavage occurs first and dehydrogenation follows a methoxy route, whereas on terrace sites, C−H cleavage occurs first and dehydrogenation follows a hydroxymethyl route.

1. INTRODUCTION

It was estimated that by 2030, the United States could produce 1.1×10^9 metric tons of dry biomass per year, which would have an energy content equivalent to 46% of the current oil consumption, if it could be properly converted into usable fuels.[1] Many publications have reported on catalytic conversion of biomass into fuels[2−26] and value-added chemicals,[11,21,26−37] with a key requirement in many of these processes being the addition of H_2. For example, fungible biofuels can be produced by pyrolysis followed by hydrodeoxygenation (HDO) of the pyrolysis oils.[38−40] At present, ways of efficiently and sustainably supplying H_2 from biomass are lacking, which impedes the expansion of biomass as a source of fuel. The catalysis research community has an important responsibility to solve this problem, so that the world can transition from oil to biofuels, which will decrease carbon emissions and improve energy independence.

Aqueous phase reforming (APR) of oxygenates converts part of the biomass to hydrogen sustainably and energy efficiently.[41−54] Specifically, oxygenates are converted over metal catalysts supported on metal oxide supports to form H_2 and CO_2; typical reaction temperatures range between 215 and 265 °C.[41,42,51,53] There are three primary steps in the APR mechanism: dehydrogenation, decarbonylation, and water−gas shift (WGS, i.e., $CO + H_2O \rightarrow CO_2 + H_2$),[43,60] as illustrated in Figure 1 for glycerol reforming over a platinum/alumina catalyst. The modest operating conditions and high chemical potential of liquid H_2O help shift the WGS equilibrium to the right ($\Delta H_r^0 = -41$ kJ/mol),[55] hence maximizing the production of H_2 and minimizing the concentration of CO, which can act as a catalyst poison, in the product stream. However, achieving high H_2 production requires designing catalysts that readily convert oxygenates to CO (and also promote WGS). As with any endeavor into catalyst design, this requires understanding the molecular-level details that control the APR mechanism. This will enable the design of catalysts that promote desired reaction pathways while keeping reactions leading to undesired byproducts to a minimum. However, a molecular-level understanding of the APR mechanism remains to be established.

Multiple groups have provided clues about how supported metal catalysts produce H_2 from oxygenates.[56−95] These studies show that the oxygenates have to undergo dehydrogenation before decarbonylation takes place and that the composition of the metal catalyst and metal oxide support

Received: April 27, 2020
Revised: July 28, 2020
Published: August 5, 2020

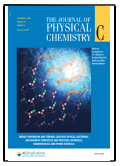

https://dx.doi.org/10.1021/acs.jpcc.0c03717
J. Phys. Chem. C 2020, 124, 19015−19023

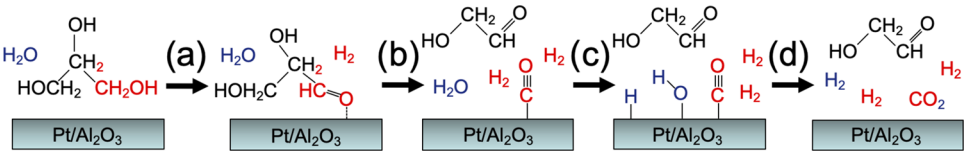

Figure 1. Simplified mechanism of aqueous phase reforming of glycerol: (a) dehydrogenation, (b) decarbonylation, (c) water dissociation (part of water−gas shift), (d) production of H_2 and CO_2 (part of water−gas shift).

strongly influence catalytic performance. Critical to understanding the mechanism is identifying the active sites. Combining results from multiple research groups collected over ∼ 15 years,[96−111] Heyden and co-workers used uncertainty quantification and microkinetic modeling to show that the active sites for the WGS step occur at the metal/support interface[112] (Figure 2). This level of molecular-

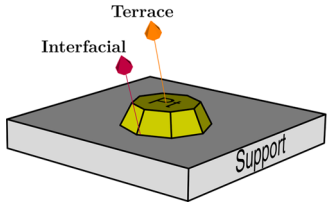

Figure 2. Cartoon illustration of catalyst sites on a supported Pt catalyst particle (yellow polyhedron) on a support (gray cuboid). The top and sides of the particle are comprised of Pt terraces, while the interfacial sites are at the boundary between the Pt cluster and the support.

level understanding does not exist for the dehydrogenation step; in fact, to our knowledge, molecular-level investigations into the mechanism of this step are limited to metal single crystals. While single-crystal studies are important for learning about the mechanism on sites likely to be located on the terraces of large metal nanoparticles (Figure 2), they cannot be extrapolated to metal/support interfaces. Hence, the role of the metal/support interface in the dehydrogenation step remains a major knowledge gap.

In this work, we use density functional theory (DFT) to calculate the thermodynamics and kinetics of methanol dehydrogenation on Pt/Al_2O_3 interfacial sites. We compare these values to analogous values previously published for Pt(111) single crystals.[113−116] We find that Pt/Al_2O_3 interfaces are active for methanol dehydrogenation, and that they promote a mechanism that is different from Pt single crystals. Specifically, methanol binds O-down to Al at Pt/Al_2O_3 interfacial sites with its hydroxyl H oriented toward Pt and its CH_3 group oriented away. Dehydrogenation thus begins with O−H cleavage and follows a methoxy (CH_3O*) route. This is in contrast to Pt(111) single crystals, where methanol binding is more amenable to C−H bond breaking, and dehydrogenation follows a hydroxymethyl (CH_2OH*) route.[116]

2. COMPUTATIONAL METHODS

2.1. Pt/Al_2O_3 Catalyst Models. Pt/Al_2O_3 interfacial sites are modeled using a Pt_4 cluster anchored at the oxygen sites[117] on an α-Al_2O_3 surface (see Figure 3 and Section S1 in the Supporting Information). The α phase of Al_2O_3 is chosen since it is computationally tractable and also because it is relatively close packed, which enables it to support a close-packed metal cluster. The Pt_4 cluster is modeled as a tetrahedron; this shape

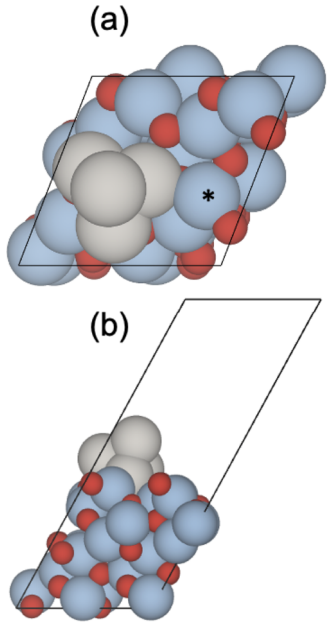

Figure 3. Top (a) and side (b) views of the Pt_4/Al_2O_3 interfacial model used in this work. Color key: oxygen = red, Al = blue, and Pt = gray. Catalytic species are adsorbed to Al that is marked with a "*" in (a). The supercell boundaries are indicated with the solid black lines.

is chosen because it is close packed, maximizing metal coordination for a four-atom cluster. Since actual catalysts comprise distributions of nanoparticle sizes, a key consideration in model development is the construction of a site where the arrangement of metal atoms at the metal/support interface could exist on a variety of cluster sizes. The tetrahedral shape with its close-packed structure is the smallest geometry that accomplishes this. The four-atom size is chosen to optimize computational tractability and chemical accuracy. Prior literature[118−122] indicates that binding energies, reaction energetics, and catalytic species geometries on four-atom metal clusters are only minorly different than the analogous values calculated on 6−10 metal-atom clusters; indeed, the binding energy of CO* (of −2.41 eV; see Table 1) calculated in this work is within the range of values calculated by Heyden and co-workers (spanning from −0.76 to −2.74 eV) on a supported Pt_8/TiO_2 cluster.[123]

An additional consideration for the development of the Pt/Al_2O_3 model is the presence of an undercoordinated Al site near the interface with Pt. Such sites exhibit Lewis acidity and promote catalytic activity.[124,125] The Pt/Al_2O_3 model employed here comprises such a site at the Pt interface, labeled with a "*" in Figure 3. For comparison, the adsorption energy of methanol at this site (of −1.21 eV; see Table 1) is within the range of values reported previously[126,127] for alcohols on Al_2O_3 surfaces (spanning from −0.43 to −2.16 eV). Further, reaction energies calculated at this site are within the range of those calculated using other models of α- and γ-

https://dx.doi.org/10.1021/acs.jpcc.0c03717
J. Phys. Chem. C 2020, 124, 19015−19023

Table 1. Calculated Reaction Energies (ΔE^{rxn}) and Activation Energies (ΔE^{act}) in eV on the Pt_4/Al_2O_3 Interfacial Model Compared with Values from ref 116 on the Pt(111) Terrace

		ΔE^{rxn} (eV)		ΔE^{act} (eV)	
	rxn.	Pt_4/Al_2O_3[a]	Pt(111)[b]	Pt_4/Al_2O_3[a]	Pt(111)[b,d]
1	CH_3OH (g) + * → CH_3OH*	−1.21	−0.46	[c]	N/A
2	CH_3OH* + * → CH_2OH* + H*	+0.35	−0.35	[c]	0.81
3	CH_2OH* + * → CHOH* + H*	−0.18	−0.29	[c]	0.73
4	CHOH* + * → COH* + H*	−0.56	−0.62	[c]	0.82
5	COH* + * → CO* + H*	−1.35	−0.49	0.65	1.23
6	CH_3OH* + * → CH_3O* + H*	−0.37	+0.50	0.30	0.87
7	CH_3O* + * → CH_2O* + H*	−0.52	−0.46	1.00	0.32
8	CH_2O* + * → CHO* + H*	−0.45	−0.75	0.84	0.39
9	CHO* + * → CO* + H*	−0.39	−1.06	1.32	0.43
10	CH_2OH* + * → CH_2O* + H*	−1.25	+0.40	[c]	0.94
11	CHOH* + * → CHO* + H*	−1.52	−0.06	[c]	0.45
12	CO* → CO (g) + *	+2.41	+1.89	[c]	N/A

[a]This work. [b]Ref 116. [c]Not calculated. [d]N/A = not available.

Al_2O_3 (see Table S2 in the Supporting Information). Further details about the selection and construction of this Pt_4/Al_2O_3 model are provided in the Supporting Information Sections S1 and S2.

The Al_2O_3 supercell employed in this work is triclinic with lattice vectors of lengths 10.3, 10.3, and 25.8 Å and angles of 55.3°. The lattice vectors are in good agreement with previously published models of α-Al_2O_3.[128−130] Al atoms on the top of one slab and those in the bottom of its adjacent vertical image are separated by over 13.5 Å. Reaction energies calculated on this slab model show only minor differences of 0.07 eV or less when compared with energies calculated on analogous slabs with extended vertical and lateral spacing (see Table S1 in the Supporting Information).

2.2. Density Functional Theory Calculations. DFT calculations are performed with the VASP code.[131−133] Exchange and correlation of valence electrons are modeled with the Perdew−Burke−Ernzerhof (PBE)[134,135] form of the generalized gradient approximation (GGA). Core electrons are modeled using projector augmented wave (PAW) pseudopotentials[132,136] to an energy cutoff of 400 eV. Gaussian smearing with a smearing factor of 0.1 eV is employed to facilitate the convergence of the electronic structures. Spin polarization is included as indicated in Section S10 in the Supporting Information. Dipole corrections are applied normal to the surface in all calculations. The D3 dispersion method[137,138] is employed to improve the modeling of dispersion interactions. Automatically generated Γ-centered Monkhorsk-Pack[139] k-point meshes of 7 × 7 × 1 are used to sample the first Brillouin zones. Electronic structure calculations are performed iteratively, and electronic structures are considered to be converged when the difference in energy between subsequent steps falls below 10^{-6} eV. Following our prior work,[140,141] energies used in this work are calculated with just one catalytic species or transition state structure in each supercell. Geometries of catalytic intermediates (local minima on the potential energy surface) are optimized using the quasi-Newton algorithm. Geometries of transition states are optimized using a combination of the climbing image nudged elastic band (CI-NEB)[142,143] and dimer[144] methods, as in prior work.[141,145] All atoms are allowed to relax in both geometry optimizations and transition state searches. Geometries are considered to be converged when the forces on all atoms fall below 0.03 eV/Å in geometry optimizations and 0.05 eV/Å in transition state searches. Transition state structures are verified via their vibrational modes, which are calculated using the center difference method. In these calculations, atoms are displaced by 0.05 Å in the + and − directions in a, b, and c dimensions. In vibrational mode calculations, the adsorbate and the atoms in the Pt_4 cluster are displaced. VASP CONTCARs for all structures considered in this work are provided in Section S10 of the Supporting Information along with the examples of the relevant INCARs (which are provided in Section S8).

3. RESULTS

3.1. Binding Geometries of Catalytic Species. Calculated adsorption geometries on the Pt_4/Al_2O_3 interfacial site models are depicted in Figure 4. For comparison, calculated adsorption geometries for the same species on Pt(111) terraces are depicted in Figures S3−S10 of the Supporting Information. On the Pt(111) terraces, CH_3OH* and CH_3O* bind via their O atoms, while CH_2OH*, CHOH*, COH*, CO*, and CHO* bind via their C atoms.[116] CH_2O* lies flat on the Pt(111) terrace. On the interfacial sites, CH_3OH* and CH_3O* bind primarily to the undercoordinated Al atom at the Pt_4/Al_2O_3 interface via their O atoms. CH_2O* and CHO* bind to the same Al atom via their O atoms and also to the Pt cluster via their C atoms. In contrast, CH_2OH*, CHOH*, COH*, and CO* bind primarily to the Pt cluster via their C atoms. The greatest differences in binding geometry on the Pt_4/Al_2O_3 interfacial sites versus the Pt(111) terraces are thus for CH_3OH*, CH_3O*, CH_2O*, and CHO*; for these species, the undercoordinated Al atom at the Pt/Al_2O_3 interface provides an additional anchoring point for the oxygenate species O atom. Indeed, CH_3OH*, CH_3O*, CH_2O*, CHO*, and CO* prefer binding at the Pt_4/Al_2O_3 interfacial sites, while CH_2OH*, CHOH*, and COH* prefer binding on the terrace sites (see Section S4 in the Supporting Information).

3.2. Calculated Thermodynamics and Kinetics. The catalytic reaction network for methanol dehydrogenation is depicted in Figure 5, and calculated energetics within this network are listed in Table 1. Reaction energies are calculated as

$$\Delta E^{rxn} = E_{CH_xOH_y*} + E_{H*} - E_{CH_{x'}OH_{y'}*} \quad (1)$$

https://dx.doi.org/10.1021/acs.jpcc.0c03717
J. Phys. Chem. C 2020, 124, 19015−19023

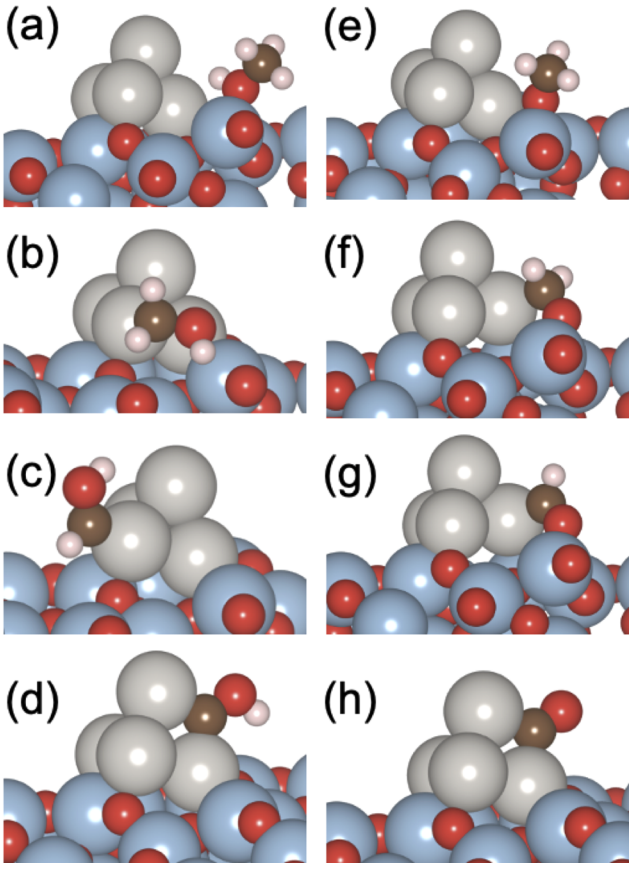

Figure 4. Calculated geometries of CH_3OH^* (a), CH_2OH^* (b), $CHOH^*$ (c), COH^* (d), CH_3O^* (e), CH_2O^* (f), CHO^* (g), and CO^* (h) on the Pt_4/Al_2O_3 interfacial sites. Color key: oxygen = red, Al = blue, Pt = gray, C = brown, H = white.

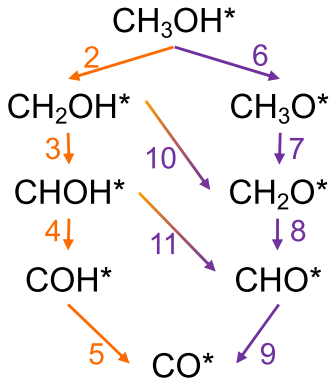

Figure 5. Possible pathways for methanol dehydrogenation. Numbers over the arrows are rxn. numbers, which are the same as in Table 1.

where $E_{CH_xOH_y*}$ and $E_{CH_{x'}OH_{y'}*}$ are calculated electronic energies (where: $(x' + y') - (x + y) = 1$; x and x' can be 0, 1, 2, or 3; and y and y' can be 0 or 1). E_{H*} is the energy of adsorbed H* on the Pt(111) surface, calculated as $E_{H*} = E_{H*}^{Pt(111)} - E_{clean}^{Pt(111)}$. We make the H* reference to Pt(111) for comparison with prior work performed on Pt(111);[116] however, the energy of H* on Pt_4/α-Al_2O_3 is identical (see the Supporting Information Section S2). Activation energies are also provided in Table 1. They are calculated as

$$\Delta E^{act} = E_{TS} - E_{reactant} \quad (2)$$

Transition state (TS) structures calculated in this work are depicted in Figures S12−S16 in the Supporting Information. We only calculate TSs for reactions that are likely to contribute to the methanol dehydrogenation mechanism, i.e., reactions that are part of dehydrogenation pathways that are thermodynamically downhill. From Table 1, this is rxns. 5−9. Molecular adsorption and desorption reactions (rxns. 1 and 12) are assumed to be unactivated.

3.3. Reaction Mechanism on the Pt_4/Al_2O_3 Interfacial versus Pt(111) Terrace Sites. The results in Table 1 show that all dehydrogenation reactions are exothermic except for rxn. 2 ($CH_3OH^* + * \rightarrow CH_2OH^* + H^*$) on the Pt_4/Al_2O_3 interfacial sites and rxns. 6 ($CH_3OH^* + * \rightarrow CH_3O^* + H^*$) and 10 ($CH_2OH^* + * \rightarrow CH_2O^* + H^*$) on the Pt(111) single-crystal terrace sites. The feasibility of surface reactions depends on their reaction free energies; estimates of the free energies of rxns. 1−12 are provided in Section S7 of the Supporting Information. Assuming a reaction temperature of 250 °C (typical of catalytic APR) and a pre-exponential factor of 10^{13} s^{-1}, reactions with $\Delta E^{act} < 1.32$ eV are kinetically facile (i.e., these reactions yield turnover frequencies of 1 s^{-1} or greater at 250 °C). All of the ΔE^{act} in Table 1 are equal to or below this value; hence, all reactions considered in this work are kinetically feasible and thus thermodynamically controlled under APR conditions. This agrees with spectroscopy analysis (see Section S5 of the Supporting Information), which indicates that CO* formation from methanol on Pt/Al_2O_3 catalysts is facile at 250 °C. Once adsorbed, methanol dehydrogenation will occur through one of four pathways (Figure 5)

- Pathway 1 (orange in Figure 4): rxn. 2 → rxn. 3 → rxn. 4 → rxn. 5
- Pathway 2 (purple in Figure 4): rxn. 6 → rxn. 7 → rxn. 8 → rxn. 9
- Pathway 3 (orange/purple in Figure 4): rxn. 2 → rxn. 10 → rxn. 8 → rxn. 9
- Pathway 4 (orange/purple in Figure 4): rxn. 2 → rxn. 3 → rxn. 11 → rxn. 9

On the Pt_4/Al_2O_3 interfacial sites, the only viable reaction pathway for methanol dehydrogenation is Pathway 2, i.e., $CH_3OH^* \rightarrow CH_3O^* \rightarrow CH_2O^* \rightarrow CHO^* \rightarrow CO^*$, since methanol dehydrogenation to hydroxymethyl (CH_2OH^*; rxn. 2) is endothermic on the Pt_4/Al_2O_3 interfacial sites. In this pathway (Pathway 2), the O−H bond is broken first, and C−H bond cleavage reactions then proceed from a methoxy (CH_3O^*) intermediate. In contrast, a C−H bond is broken first on the Pt(111) terraces, and methanol dehydrogenation proceeds via a hydroxymethyl (CH_2OH^*) intermediate.[116] Taken together, these results indicate that the pathway for methanol dehydrogenation depends on the site where methanol adsorbs, following a methoxy route if adsorbed to a Pt/Al_2O_3 interfacial site and a hydroxymethyl route if adsorbed to a Pt(111) terrace site.

4. DISCUSSION

The preference for the methoxy route on the interfacial sites is motivated by the thermodynamic preference of species with cleaved O−H bonds and/or fully saturated methyl groups to bind to Lewis acid sites. Specifically, CH_3OH^*, CH_3O^*, CH_2O^*, and CHO^* bind strongly to the undercoordinated Al ion at the Pt interface via their O atoms (CH_2O^* and CHO^* also bind to the Pt_4 cluster via their C atoms). In contrast,

https://dx.doi.org/10.1021/acs.jpcc.0c03717
J. Phys. Chem. C 2020, 124, 19015−19023

CH_2OH*, CHOH*, COH*, and CO* bind to the Pt_4 particle and interact minimally with the Al_2O_3 support. The step where methanol fragments transition from utilizing Lewis acid sites at the Pt/Al_2O_3 interface to binding to Pt is CHO* + * → CO* + H*; breaking the HCO−Al bond in this reaction invokes a large kinetic barrier.

The reaction CH_3O* + * → CH_2O* + H* also has a high barrier. Comparing the structure of the methoxy intermediate in Figure 3e to the transition state for CH_3O* + * → CH_2O* + H* in Figure S14, this reaction requires CH_3O* to reorient from its preferred structure, which has the methyl group pointing away from the Pt particle. CH_3OH* also takes on a geometry where the methyl group is oriented away from the Pt particle (see Figure 3a); indeed, breaking a C−H bond to form CH_2OH* is endothermic. Hence, in addition to providing Lewis acid sites that strengthen binding of oxygenates with cleaved O−H bonds and/or fully saturated methyl groups, Pt/Al_2O_3 interfacial sites additionally serve to orient oxygenates to favor O−H cleavage and hinder C−H cleavage. We expect that this phenomenon will be even more significant for larger oxygenates that can interact with multiple support sites,[146,147] which could help to explain the decreasing H_2 yield in APR with increasing size of the feed molecule.[41,148] We will investigate such phenomena in detail in future work.

5. CONCLUSIONS

In this work, we have used DFT calculations to learn about the sites for methanol dehydrogenation on Pt/Al_2O_3 catalysts. Methanol binds exothermically to Pt(111) terraces and Pt_4/Al_2O_3 interfaces; however, methanol adsorption at Pt_4/Al_2O_3 interfaces is significantly stronger due to a favorable interaction with Lewis acid sites on the Al_2O_3 support. Methanol bound to Pt_4/Al_2O_3 interfaces is converted via O−H cleavage to methoxy, which is then converted to CO* via subsequent C−H cleavage steps. All CH_xO* species along this pathway retain the O−Al bond except CO*; breaking the O−Al bond in the reaction CHO* + * → CO* + H* has a large kinetic barrier. In contrast, methanol bound to Pt(111) terraces is converted via C−H cleavage to hydroxymethyl. Significant if not full C−H cleavage is then achieved before the O−H bond is broken.[116] Hydroxymethyl (CH_2OH*) and its derivatives (CHOH*, COH*) interact minimally with the Al_2O_3 support; in contrast, species with fully saturated methyl groups (CH_3OH*, CH_3O*) bind strongly to the Al_2O_3 support and interact minimally with the Pt_4 cluster. With the exception of CO*, species with incompletely saturated methyl groups and broken O−H bonds (CH_2O*, CHO*) bind to the Al_2O_3 support via their O atoms and the Pt_4 cluster via their C atoms. CO* prefers binding to the Pt particle and interacts minimally with the Al_2O_3 support.

While the results presented here provide insight about the active sites for methanol dehydrogenation on Pt/Al_2O_3 catalysts in the vapor phase, APR is carried out in aqueous phase, and water will almost assuredly change the chemical picture. For example, we have previously shown that liquid water significantly influences the reaction energies and mechanisms of O−H cleavage reactions in the pathway for methanol dehydrogenation,[140] making reaction energies more positive (due to a decrease in hydrophilicity of the catalytic species) and decreasing activation energies to 0 (by acting as a cocatalyst). Further, liquid water and its fragments can compete with methanol and its fragments for catalytic sites,[149] including hydrating the Al_2O_3 surface.[146,147] Further, water is likely to interact strongly with a polar support such as Al_2O_3 and this competition could drive the reaction toward non-interfacial sites. One of our immediate next steps is to begin clarifying the influence of liquid water on the dehydrogenation step in APR at metal/support interfaces; understanding the reaction pathway in the vapor phase is a necessary first step.[140,150]

■ ASSOCIATED CONTENT

Supporting Information

The Supporting Information is available free of charge at https://pubs.acs.org/doi/10.1021/acs.jpcc.0c03717.

Illustrations of structures not included in the main text, all input parameters for simulations, structure files for all species considered in this work, details about the bulk Al_2O_3 model, comparisons of energetics with other Al_2O_3 models, thermochemistry calculations, spectroscopy results (PDF)

■ AUTHOR INFORMATION

Corresponding Author

Rachel B. Getman − *Department of Chemical and Biomolecular Engineering, Clemson University, Clemson, South Carolina 29634-0909, United States;* orcid.org/0000-0003-0755-0534; Email: rgetman@g.clemson.edu

Authors

Tianjun Xie − *Department of Chemical and Biomolecular Engineering, Clemson University, Clemson, South Carolina 29634-0909, United States*

Bryan J. Hare − *Department of Chemical and Biomolecular Engineering, Georgia Institute of Technology, Atlanta, Georgia 30332, United States*

Paul J. Meza-Morales − *Department of Chemical and Biomolecular Engineering, Clemson University, Clemson, South Carolina 29634-0909, United States*

Carsten Sievers − *Department of Chemical and Biomolecular Engineering, Georgia Institute of Technology, Atlanta, Georgia 30332, United States*

Complete contact information is available at: https://pubs.acs.org/10.1021/acs.jpcc.0c03717

Notes

The authors declare no competing financial interest.

■ ACKNOWLEDGMENTS

This research was funded by the National Science Foundation under award numbers CHE-1764296 and CHE-1764304. Simulations were performed on the Palmetto Supercomputing Cluster, which is maintained by the Cyberinfrastructure Technology Integration Group at Clemson University. The authors thank Ricardo García Cáramco (Clemson University Department of Chemical and Biomolecular Engineering) for helping to validate the Pt_4/Al_2O_3 model used in this work and Stephen Vicchio (Clemson University Department of Chemical and Biomolecular Engineering) for help with the gas phase thermochemistry.

■ REFERENCES

(1) Park Ovard, L.; Ulrich, T. H.; Muth, D. J.; Hess, J. R.; Thomas, S.; Stokes, B. *U.S. Billion-Ton Update: Biomass Supply for a Bioenergy*

and Bioproducts Industry; Oak Ridge National Lab: Oak Ridge, TN, 2011.
(2) Huber, G. W.; Dumesic, J. A. An Overview of Aqueous-Phase Catalytic Processes for Production of Hydrogen and Alkanes in a Biorefinery. *Catal. Today* **2006**, *111*, 119−132.
(3) Huber, G. W.; Iborra, S.; Corma, A. Synthesis of Transportation Fuels from Biomass: Chemistry, Catalysts, and Engineering. *Chem. Rev.* **2006**, *106*, 4044−4098.
(4) Bell, A. T.; Gates, B. C.; Ray, D. *Catalysis for Energy*, PNNL-17214, U.S. Department of Energy Basic Energy Sciences Workshop Report; U.S. Department of Energy, 2008.
(5) Vispute, T. P.; Huber, G. W. *Breaking the Chemical and Engineering Barriers to Lignocellulosic Biofuels: Next Generation Hydrocarbon Biorefineries*; National Science Foundation: Washington D.C., 2007; 138−149.
(6) Hayes, D. J. An Examination of Biorefining Processes, Catalysts and Challenges. *Catal. Today* **2009**, *145*, 138−151.
(7) Ohlrogge, J.; Allen, D.; Berguson, B.; DellaPenna, D.; Shachar-Hill, Y.; Stymne, S. Driving on Biomass. *Science* **2009**, *324*, 1019−1020.
(8) Willems, P. A. The Biofuels Landscape through the Lens of Industrial Chemistry. *Science* **2009**, *325*, 707−708.
(9) Regalbuto, J. R. Cellulosic Biofuels - Got Gasoline? *Science* **2009**, *325*, 822−824.
(10) Adjaye, J. D.; Bakhshi, N. N. Catalytic Conversion of a Biomass-Derived Oil to Fuels and Chemicals 1. Model-Compound Studies and Reaction Pathways. *Biomass Bioenergy* **1995**, *8*, 131−149.
(11) Alonso, D. M.; Wettstein, S. G.; Dumesic, J. A. Bimetallic Catalysts for Upgrading of Biomass to Fuels and Chemicals. *Chem. Soc. Rev.* **2012**, *41*, 8075−8098.
(12) Balat, M.; Kirtay, E.; Balat, H.; Balat, M. Main Routes for the Thermo-Conversion of Biomass into Fuels and Chemicals. Part 1: Pyrolysis Systems. *Energy Conv. Manag.* **2009**, *50*, 3147−3157.
(13) Braden, D. J.; Henao, C. A.; Heltzel, J.; Maravelias, C. T.; Dumesic, J. A. Production of Liquid Hydrocarbon Fuels by Catalytic Conversion of Biomass-Derived Levulinic Acid. *Green Chem.* **2011**, *13*, 1755−1765.
(14) Bulushev, D. A.; Ross, J. R. H. Catalysis for Conversion of Biomass to Fuels Via Pyrolysis and Gasification: A Review. *Catal. Today* **2011**, *171*, 1−13.
(15) Chheda, J. N.; Huber, G. W.; Dumesic, J. A. Liquid-Phase Catalytic Processing of Biomass-Derived Oxygenated Hydrocarbons to Fuels and Chemicals. *Angew. Chem., Int. Ed.* **2007**, *46*, 7164−7183.
(16) French, R.; Czernik, S. Catalytic Pyrolysis of Biomass for Biofuels Production. *Fuel Process. Technol.* **2010**, *91*, 25−32.
(17) Huber, G. W.; Corma, A. Synergies between Bio- and Oil Refineries for the Production of Fuels from Biomass. *Angew. Chem., Int. Ed.* **2007**, *46*, 7184−7201.
(18) Lappas, A. A.; Samolada, M. C.; Iatridis, D. K.; Voutetakis, S. S.; Vasalos, I. A. Biomass Pyrolysis in a Circulating Fluid Bed Reactor for the Production of Fuels and Chemicals. *Fuel* **2002**, *81*, 2087−2095.
(19) Larson, E. D.; Fiorese, G.; Liu, G. J.; Williams, R. H.; Kreutz, T. G.; Consonni, S. Co-Production of Decarbonized Synfuels and Electricity from Coal Plus Biomass with CO2 Capture and Storage: An Illinois Case Study. *Energy Environ. Sci.* **2010**, *3*, 28−42.
(20) Serrano-Ruiz, J. C.; Pineda, A.; Balu, A. M.; Luque, R.; Campelo, J. M.; Romero, A. A.; Ramos-Fernandez, J. M. Catalytic Transformations of Biomass-Derived Acids into Advanced Biofuels. *Catal. Today* **2012**, *195*, 162−168.
(21) Sheldon, R. A. Utilisation of Biomass for Sustainable Fuels and Chemicals: Molecules, Methods and Metrics. *Catal. Today* **2011**, *167*, 3−13.
(22) Simonetti, D. A.; Dumesic, J. A. Catalytic Production of Liquid Fuels from Biomass-Derived Oxygenated Hydrocarbons: Catalytic Coupling at Multiple Length Scales. *Catal. Rev.* **2009**, *51*, 441−484.
(23) Stöcker, M. Biofuels and Biomass-to-Liquid Fuels in the Biorefinery: Catalytic Conversion of Lignocellulosic Biomass Using Porous Materials. *Angew. Chem., Int. Ed.* **2008**, *47*, 9200−9211.
(24) Thangalazhy-Gopakumar, S.; Adhikari, S.; Gupta, R. B.; Tu, M. B.; Taylor, S. Production of Hydrocarbon Fuels from Biomass Using Catalytic Pyrolysis under Helium and Hydrogen Environments. *Bioresour. Technol.* **2011**, *102*, 6742−6749.
(25) Yaman, S. Pyrolysis of Biomass to Produce Fuels and Chemical Feedstocks. *Energy Conv. Manage.* **2004**, *45*, 651−671.
(26) Zhou, C. H.; Xia, X.; Lin, C. X.; Tong, D. S.; Beltramini, J. Catalytic Conversion of Lignocellulosic Biomass to Fine Chemicals and Fuels. *Chem. Soc. Rev.* **2011**, *40*, 5588−5617.
(27) Corma, A.; Iborra, S.; Velty, A. Chemical Routes for the Transformation of Biomass into Chemicals. *Chemical Reviews* **2007**, *107*, 2411−2502.
(28) Werpy, T.; Petersen, G. *Top Value Added Chemicals from Biomass: Vol. 1—Results of Screening for Potential Candidates from Sugars and Synthesis Gas*, NREL/TP-510-35523; National Renewable Energy Laboratory: Golden, CO, 2004.
(29) Casanova, O.; Iborra, S.; Corma, A. Biomass into Chemicals: One Pot-Base Free Oxidative Esterification of 5-Hydroxymethyl-2-Furfural into 2,5-Dimethylfuroate with Gold on Nanoparticulated Ceria. *J. Catal.* **2009**, *265*, 109−116.
(30) Casanova, O.; Iborra, S.; Corma, A. Biomass into Chemicals: Aerobic Oxidation of 5-Hydroxymethyl-2-Furfural into 2,5-Furandicarboxylic Acid with Gold Nanoparticle Catalysts. *ChemSusChem* **2009**, *2*, 1138−1144.
(31) Climent, M. J.; Corma, A.; De Frutos, P.; Iborra, S.; Noy, M.; Velty, A.; Concepcion, P. Chemicals from Biomass: Synthesis of Glycerol Carbonate by Transesterification and Carbonylation with Urea with Hydrotalcite Catalysts. The Role of Acid-Base Pairs. *J. Catal.* **2010**, *269*, 140−149.
(32) Climent, M. J.; Corma, A.; Hamid, S. B. A.; Iborra, S.; Mifsud, M. Chemicals from Biomass Derived Products: Synthesis of Polyoxyethyleneglycol Esters from Fatty Acid Methyl Esters with Solid Basic Catalysts. *Green Chem.* **2006**, *8*, 524−532.
(33) Corma, A.; Huber, G. W.; Sauvanauda, L.; O'Connor, P. Biomass to Chemicals: Catalytic Conversion of Glycerol/Water Mixtures into Acrolein, Reaction Network. *J. Catal.* **2008**, *257*, 163−171.
(34) Hick, S. M.; Griebel, C.; Restrepo, D. T.; Truitt, J. H.; Buker, E. J.; Bylda, C.; Blair, R. G. Mechanocatalysis for Biomass-Derived Chemicals and Fuels. *Green Chem.* **2010**, *12*, 468−474.
(35) Lipinsky, E. S. Chemicals from Biomass - Petrochemical Substitution Options. *Science* **1981**, *212*, 1465−1471.
(36) Mäki-Arvela, P.; Holmbom, B.; Salmi, T.; Murzin, D. Y. Recent Progress in Synthesis of Fine and Specialty Chemicals from Wood and Other Biomass by Heterogeneous Catalytic Processes. *Catal. Rev.* **2007**, *49*, 197−340.
(37) van Haveren, J.; Scott, E. L.; Sanders, J. Bulk Chemicals from Biomass. *Biofuels Bioprod. Bioref.* **2008**, *2*, 41−57.
(38) Elliott, D. C. Historical Developments in Hydroprocessing Bio-Oils. *Energy Fuels* **2007**, *21*, 1792−1815.
(39) Furimsky, E. Catalytic Hydrodeoxygenation. *Appl. Catal., A* **2000**, *199*, 147−190.
(40) Hicks, J. C. Advances in C-O Bond Transformations in Lignin-Derived Compounds for Biofuels Production. *J. Phys. Chem. Lett.* **2011**, *2*, 2280−2287.
(41) Cortright, R. D.; Davda, R. R.; Dumesic, J. A. Hydrogen from Catalytic Reforming of Biomass-Derived Hydrocarbons in Liquid Water. *Nature* **2002**, *418*, 964−967.
(42) Davda, R. R.; Dumesic, J. A. Catalytic Reforming of Oxygenated Hydrocarbons for Hydrogen with Low Levels of Carbon Monoxide. *Angew. Chem., Int. Ed.* **2003**, *42*, 4068−4071.
(43) Davda, R. R.; Shabaker, J. W.; Huber, G. W.; Cortright, R. D.; Dumesic, J. A. Aqueous-Phase Reforming of Ethylene Glycol on Silica-Supported Metal Catalysts. *Appl. Catal., B* **2003**, *43*, 13−26.
(44) Shabaker, J. W.; Huber, G. W.; Davda, R. R.; Cortright, R. D.; Dumesic, J. A. Aqueous-Phase Reforming of Ethylene Glycol over Supported Platinum Catalysts. *Catal. Lett.* **2003**, *88*, 1−8.
(45) King, D. L.; Zhang, L. A.; Xia, G.; Karim, A. M.; Heldebrant, D. J.; Wang, X. Q.; Peterson, T.; Wang, Y. Aqueous Phase Reforming of

https://dx.doi.org/10.1021/acs.jpcc.0c03717
J. Phys. Chem. C 2020, 124, 19015−19023

Glycerol for Hydrogen Production over Pt-Re Supported on Carbon. *Appl. Catal., B* **2010**, *99*, 206−213.
(46) Kim, T. W.; Kim, H. D.; Jeong, K. E.; Chae, H. J.; Jeong, S. Y.; Lee, C. H.; Kim, C. U. Catalytic Production of Hydrogen through Aqueous-Phase Reforming over Platinum/Ordered Mesoporous Carbon Catalysts. *Green Chem.* **2011**, *13*, 1718−1728.
(47) Manfro, R. L.; da Costa, A. F.; Ribeiro, N. F. P.; Souza, M. Hydrogen Production by Aqueous-Phase Reforming of Glycerol over Nickel Catalysts Supported on CeO_2. *Fuel Process. Technol.* **2011**, *92*, 330−335.
(48) Menezes, A. O.; Rodrigues, M. T.; Zimmaro, A.; Borges, L. E. P.; Fraga, M. A. Production of Renewable Hydrogen from Aqueous-Phase Reforming of Glycerol over Pt Catalysts Supported on Different Oxides. *Renew.able Energy* **2011**, *36*, 595−599.
(49) Shabaker, J. W.; Dumesic, J. A. Kinetics of Aqueous-Phase Reforming of Oxygenated Hydrocarbons: Pt/Al_2O_3 and Sn-Modified Ni Catalysts. *Ind. Eng. Chem. Res.* **2004**, *43*, 3105−3112.
(50) Shabaker, J. W.; Huber, G. W.; Dumesic, J. A. Aqueous-Phase Reforming of Oxygenated Hydrocarbons over Sn-Modified Ni Catalysts. *J. Catal.* **2004**, *222*, 180−191.
(51) Luo, N. J.; Fu, X. W.; Cao, F. H.; Xiao, T. C.; Edwards, P. P. Glycerol Aqueous Phase Reforming for Hydrogen Generation over Pt Catalyst - Effect of Catalyst Composition and Reaction Conditions. *Fuel* **2008**, *87*, 3483−3489.
(52) Huber, G. W.; Cortright, R. D.; Dumesic, J. A. Renewable Alkanes by Aqueous-Phase Reforming of Biomass-Derived Oxygenates. *Angew. Chem., Int. Ed.* **2004**, *43*, 1549−1551.
(53) Huber, G. W.; Shabaker, J. W.; Dumesic, J. A. Raney Ni-Sn Catalyst for H2 Production from Biomass-Derived Hydrocarbons. *Science* **2003**, *300*, 2075−2077.
(54) Huber, G. W.; Shabaker, J. W.; Evans, S. T.; Dumesic, J. A. Aqueous-Phase Reforming of Ethylene Glycol over Supported Pt and Pd Bimetallic Catalysts. *Appl. Catal., B* **2006**, *62*, 226−235.
(55) Wheeler, C.; Jhalani, A.; Klein, E. J.; Tummala, S.; Schmidt, L. D. The Water-Gas-Shift Reaction at Short Contact Times. *J. Catal.* **2004**, *223*, 191−199.
(56) Tupy, S. A.; Karim, A. M.; Bagia, C.; Deng, W.; Huang, Y.; Vlachos, D. G.; Chen, J. G. Correlating Ethylene Glycol Reforming Activity with in Situ Exafs Detection of Ni Segregation in Supported NiPt Bimetallic Catalysts. *ACS Catal.* **2012**, *2*, 2290−2296.
(57) Stottlemyer, A. L.; Ren, H.; Chen, J. G. Reactions of Methanol and Ethylene Glycol on Ni/Pt: Bridging the Materials Gap between Single Crystal and Polycrystalline Bimetallic Surfaces. *Surf. Sci.* **2009**, *603*, 2630−2638.
(58) Skoplyak, O.; Menning, C. A.; Barteau, M. A.; Chen, J. G. Reforming of Oxygenates for H2 Production on 3d/Pt(111) Bimetallic Surfaces. *Top. Catal.* **2008**, *51*, 49−59.
(59) Skoplyak, O.; Menning, C. A.; Barteau, M. A.; Chen, J. G. Experimental and Theoretical Study of Reactivity Trends for Methanol on Co/Pt(111) and Ni/Pt(111) Bimetallic Surfaces. *J. Chem. Phys.* **2007**, *127*, No. 114707.
(60) Skoplyak, O.; Barteau, M. A.; Chen, J. G. Reforming of Oxygenates for H2 Production: Correlating Reactivity of Ethylene Glycol and Ethanol on Pt(111) and Ni/Pt(111) with Surface d-Band Center. *J. Phys. Chem. B* **2006**, *110*, 1686−1694.
(61) Skoplyak, O.; Barteau, M. A.; Chen, J. G. Ethanol and Ethylene Glycol on Ni/Pt(111) Bimetallic Surfaces: A DFT and HREELS Study. *Surf. Sci.* **2008**, *602*, 3578−3587.
(62) Skoplyak, O.; Barteau, M. A.; Chen, J. G. Comparison of H2 Production from Ethanol and Ethylene Glycol on M/Pt(111) (M = Ni, Fe, Ti) Bimetallic Surfaces. *Catal. Today* **2009**, *147*, 150−157.
(63) Salciccioli, M.; Yu, W.; Barteau, M. A.; Chen, J. G.; Vlachos, D. G. Differentiation of O-H and C-H Bond Scission Mechanisms of Ethylene Glycol on Pt and Ni/Pt Using Theory and Isotopic Labeling Experiments. *J. Am. Chem. Soc.* **2011**, *133*, 7996−8004.
(64) McManus, J. R.; Salciccioli, M.; Yu, W.; Vlachos, D. G.; Chen, J. G.; Vohs, J. M. Correlating the Surface Chemistry of C2 and C3 Aldoses with a C6 Sugar: Reaction of Glucose, Glyceraldehyde, and Glycoaldehyde on Pd(111). *J. Phys. Chem. C* **2012**, *116*, 18891−18898.
(65) Salciccioli, M.; Vlachos, D. G. Kinetic Modeling of Pt Catalyzed and Computation-Driven Catalyst Discovery for Ethylene Glycol Decomposition. *ACS Catal.* **2011**, *10*, 1246−1256.
(66) Chen, Y.; Salciccioli, M.; Vlachos, D. G. An Efficient Reaction Pathway Search Method Applied to the Decomposition of Glycerol on Platinum. *J. Phys. Chem. C* **2011**, *115*, 18707−18720.
(67) Caglar, B.; Ozbek, M. O.; Niemantsverdriet, J. W. H.; Weststrate, C. J. K.-J. Modeling the Surface Chemistry of Sugars: Glycoaldehyde on Rhodium (100). *J. Phys. Chem. C* **2015**, *119*, 22915−22923.
(68) Gu, X.-K.; Liu, B.; Greeley, J. First-Principles Study of Structure Sensitivity of Ethylene Glycol Conversion on Platinum. *ACS Catal.* **2015**, *5*, 2623−2631.
(69) Lv, C.-Q.; Yang, B.; Pang, X.-Y.; Wang, G.-C. Reaction Mechanism of Ethylene Glycol Decomposition on Pt Model Catalysts: A Density Functional Theory Study. *Appl. Surf. Sci.* **2016**, *390*, 1015−1022.
(70) de Vlieger, D. J. M.; Mojet, B. L.; Lefferts, L.; Seshan, K. Aqueous Phase Reforming of Ethylene Glycol - Role of Intermediates in Catalyst Performance. *J. Catal.* **2012**, *292*, 239−245.
(71) Kandoi, S.; Greeley, J.; Sanchez-Castillo, M. A.; Evans, S. T.; Gokhale, A. A.; Dumesic, J. A.; Mavrikakis, M. Prediction of Experimental Methanol Decomposition Rates on Platinum from First Principles. *Top. Catal.* **2006**, *37*, 17−28.
(72) Mavrikakis, M.; Barteau, M. A. Oxygenate Reaction Pathways on Transition Metal Surfaces. *J. Mol. Catal. A: Chem.* **1998**, *131*, 135−147.
(73) Alcalá, R.; Mavrikakis, M.; Dumesic, J. A. DFT Studies for Cleavage of C-C and C-O Bonds in Surface Species Derived from Ethanol on Pt(111). *J. Catal.* **2003**, *218*, 178−190.
(74) Salciccioli, M.; Chen, Y.; Vlachos, D. G. Density Functional Theory-Derived Group Additivity and Linear Scaling Methods for Prediction of Oxygenate Stability on Metal Catalysts: Adsorption of Open-Ring Alcohol and Polyol Dehydrogenation Intermediates on Pt-Based Metals. *J. Phys. Chem. C* **2010**, *114*, 20155−20166.
(75) Kandoi, S.; Greeley, J.; Simonetti, D.; Shabaker, J.; Dumesic, J. A.; Mavrikakis, M. Reaction Kinetics of Ethylene Glycol Reforming over Platinum in the Vapor Versus Aqueous Phases. *J. Phys. Chem. C* **2011**, *115*, 961−971.
(76) Liu, B.; Greeley, J. Density Functional Theory Study of Selectivity Considerations for C-C Versus C-O Bond Scission in Glycerol Decomposition on Pt(111). *Top. Catal.* **2012**, *55*, 280−289.
(77) Auneau, F.; Michel, C.; Delbecq, F.; Pinel, C.; Sautet, P. Unravelling the Mechanism of Glycerol Hydrogenolysis over Rhodium Catalyst through Combined Experimental-Theoretical Investigations. *Chem. Eur. J.* **2011**, *17*, 14288−14299.
(78) Coll, D.; Delbecq, F.; Aray, Y.; Sautet, P. Stability of Intermediates in the Glycerol Hydrogenolysis on Transition Metal Catalysts from First Principles. *Phys. Chem. Chem. Phys.* **2011**, *13*, 1448−1456.
(79) Simonetti, D. A.; Kunkes, E. L.; Dumesic, J. A. Gas-Phase Conversion of Glycerol to Synthesis Gas over Carbon-Supported Platinum and Platinum-Rhenium Catalysts. *J. Catal.* **2007**, *247*, 298−306.
(80) Liu, B.; Greeley, J. A Density Functional Theory Analysis of Trends in Glycerol Decomposition on Close-Packed Transition Metal Surfaces. *Phys. Chem. Chem. Phys.* **2013**, *15*, 6475−6485.
(81) Liu, B.; Zhou, M.; Chan, M. K. Y.; Greeley, J. P. Understanding Polyol Decomposition on Bimetallic Pt-Mo Catalysts-A DFT Study of Glycerol. *ACS Catal.* **2015**, *5*, 4942−4950.
(82) Xie, T.; Bodenschatz, C. J.; Getman, R. B. Insights into the Roles of Water on the Aqueous Phase Reforming of Glycerol. *React. Chem. Eng.* **2019**, *4*, 383−392.
(83) Shan, N.; Liu, B. Elucidating Molecular Interactions in Glycerol Adsorption at the Metal-Water Interface with Density Functional Theory. *Langmuir* **2019**, *35*, 4791−4805.

https://dx.doi.org/10.1021/acs.jpcc.0c03717
J. Phys. Chem. C 2020, 124, 19015−19023

(84) Li, Q.; García-Muelas, R.; López, N. Microkinetics of Alcohol Reforming for H2 Production from a Fair Density Functional Theory Database. *Nat. Commun.* **2018**, *9*, No. 526.
(85) García-Muelas, R.; López, N. Collective Descriptors for the Adsorption of Sugar Alcohols on Pt and Pd(111). *J. Phys. Chem. C* **2014**, *118*, 17531−17537.
(86) Garcia-Ratés, M.; García-Muelas, R.; López, N. Solvation Effects on Methanol Decomposition on Pd(111), Pt(111), and Ru(0001). *J. Phys. Chem. C* **2017**, *121*, 13803−13809.
(87) Faheem, M.; Saleheen, M.; Lu, J.; Heyden, A. Ethylene Glycol Reforming on Pt(111): First-Principles Microkinetic Modeling in Vapor and Aqueous Phases. *Catal. Sci. Technol.* **2016**, *6*, 8242−8256.
(88) Zaffran, J.; Michel, C.; Delbecq, F.; Sautet, P. Towards More Accurate Prediction of Activation Energies for Polyalcohol Dehydrogenation on Transition Metal Catalysts in Water. *Catal. Sci. Technol.* **2016**, *6*, 6615−6624.
(89) Baltrusaitis, J.; Valter, M.; Hellman, A. Geometry and Electronic Properties of Glycerol Adsorbed on Bare and Transition-Metal Surface-Alloyed Au(111): A Density Functional Theory Study. *J. Phys. Chem. C* **2016**, *120*, 1749−1757.
(90) Amaral, R. C.; Tereshchuk, P.; Seminovski, Y.; Da Silva, J. L. F. The Role of Low-Coordinated Sites on the Adsorption of Glycerol on Defected Ptn/Pt(111) Substrates: A Density Functional Investigation within the D3 Van Der Waals Correction. *J. Phys. Chem. C* **2017**, *121*, 3445−3454.
(91) Tereshchuk, P.; Amaral, R. C.; Seminovski, Y.; Da Silva, J. L. F. Glycerol Adsorption on a Defected Pt6/Pt(100) Substrate: A Density Functional Theory Investigation within the D3 Van Der Waals Correction. *RSC Adv.* **2017**, *7*, 17122−17127.
(92) Costa-Amaral, R.; Da Silva, J. L. F. The Adsorption of Alcohols on Strained Pt3Ni(111) Substrates: A Density Functional Investigation within the D3 Van Der Waals Correction. *Phys. Chem. Chem. Phys.* **2018**, *20*, 24210−24221.
(93) Calderón, L. A.; Montoya, A.; Soon, A.; Stampfl, C. Non-Dissociative Adsorption of Glycerol on the (111) Surface of Ni and Pt-Based Metallic Systems: Hints on Reforming Activity from D-Band Center. *Mol. Catal.* **2019**, *474*, No. 110412.
(94) Mendes, P. C. D.; Costa-Amaral, R.; Gomes, J. F.; Da Silva, J. L. F. The Influence of Hydroxy Groups on the Adsorption of Three-Carbon Alcohols on Ni(111), Pd(111) and Pt(111) Surfaces: A Density Functional Theory Study within the D3 Dispersion Correction. *Phys. Chem. Chem. Phys.* **2019**, *21*, 8434−8444.
(95) Gu, G. H.; Wittreich, G. R.; Vlachos, D. G. Microkinetic Modeling of Aqueous Phase Biomass Conversion: Application to Ethylene Glycol Reforming. *Chem. Eng. Sci.* **2019**, *197*, 415−418.
(96) Grabow, L. C.; Gokhale, A. A.; Evans, S. T.; Dumesic, J. A.; Mavrikakis, M. Mechanism of the Water Gas Shift Reaction on Pt: First Principles, Experiments, and Microkinetic Modeling. *J. Phys. Chem. C* **2008**, *112*, 4608−4617.
(97) Stamatakis, M.; Chen, Y.; Vlachos, D. G. First-Principles-Based Kinetic Monte Carlo Simulation of the Structure Sensitivity of the Water-Gas Shift Reaction on Platinum Surfaces. *J. Phys. Chem. C* **2011**, *115*, 24750−24762.
(98) Stamatakis, M.; Vlachos, D. G. A Graph-Theoretical Kinetic Monte Carlo Framework for on-Lattice Chemical Kinetics. *J. Chem. Phys.* **2011**, *134*, No. 214115.
(99) Clay, J. P.; Greeley, J. P.; Ribeiro, F. H.; Delgass, W. N.; Schneider, W. F. DFT Comparison of Intrinsic WGS Kinetics over Pd and Pt. *J. Catal.* **2014**, *320*, 106−117.
(100) Azzam, K. G.; Babich, I. V.; Seshan, K.; Lefferts, L. Bifunctional Catalysts for Single-Stage Water-Gas Shift Reaction in Fuel Cell Applications: Part 1. Effect of the Support on the Reaction Sequence. *J. Catal.* **2007**, *251*, 153−162.
(101) Kalamaras, C. M.; Panagiotopoulou, P.; Kondarides, D. I.; Efstathiou, A. M. Kinetic and Mechanistic Studies of the Water-Gas Shift Reaction on Pt/TiO2 Catalyst. *J. Catal.* **2009**, *264*, 117−129.
(102) Thinon, O.; Rachedi, K.; Diehl, F.; Avenier, P.; Schuurman, Y. Kinetics and Mechanism of the Water-Gas Shift Reaction over Platinum Supported Catalysts. *Top. Catal.* **2009**, *52*, 1940−1945.
(103) Pazmiño, J. H.; Shekhar, M.; Williams, W. D.; Akatay, M. C.; Miller, J. T.; Delgass, W. N.; Ribeiro, F. H. Metallic Pt as Active Sites for the Water-Gas Shift Reaction on Alkali-Promoted Supported Catalysts. *J. Catal.* **2012**, *286*, 279−286.
(104) Mudiyanselage, K.; Senanayake, S. D.; Feria, L.; Shankhamala, K.; Baber, A. E.; Graciani, J.; Vidal, A. B.; Agnoli, S.; Evans, J.; Chang, R.; Axnanda, S.; Liu, Z.; Sanz, J. F.; Liu, P.; Rodriguez, J. A.; Stacchiola, D. J. Importance of the Metal-Oxide Interface in Catalysis: In Situ Studies of the Water-Gas Shift Reaction by Ambient-Pressure X-Ray Photoelectron Spectroscopy. *Angew. Chem., Int. Ed.* **2013**, *52*, 5101−5105.
(105) Bruix, A.; Rodrigues, J. A.; Ramírez, P. J.; Senanayake, S. D.; Evans, J.; Park, J. B.; Stacchiola, D.; Liu, P.; Hrbek, J.; Illas, F. A. A New Type of Strong Metal-Support Interaction and the Production of H2 through the Transformation of Water on Pt/CeO2(111) and Pt/CeOx/TiO2(110) Catalysts. *J. Am. Chem. Soc.* **2012**, *134*, 8968−8974.
(106) Ding, K.; Gulec, A.; Johnson, A. M.; Schweitzer, N. M.; Stucky, G. D.; Marks, L. D.; Stair, P. C. Identification of Active Sites in CO Oxidation and Water-Gas Shift over Supported Pt Catalysts. *Science* **2015**, *350*, 189.
(107) Fu, Q.; Saltsburg, H.; Flytzani-Stephanopoulos, M. Active Nonmetallic Au and Pt Species on Ceria-Based Water-Gas Shift Catalysts. *Science* **2003**, *301*, 935−938.
(108) Yang, M.; Liu, J.; Lee, S.; Zugic, B.; Huang, J.; Allard, L. F.; Flytzani-Stephanopoulos, M. A Common Single-Site Pt(II)-O(OH)-X- Species Stabilized by Sodium on "Active" and "Inert" Supports Catalyzes the Water-Gas Shift Reaction. *J. Am. Chem. Soc.* **2015**, *137*, 3470−3473.
(109) Ammal, S.; Heyden, A. Water-Gas Shift Activity of Atomically Dispersed Cationic Platinum Versus Metallic Platinum Clusters on Titania Supports. *ACS Catal.* **2017**, *7*, 301−309.
(110) Walker, E.; Ammal, S. C.; Terejanu, G. A.; Heyden, A. Uncertainty Quantification Framework Applied to the Water-Gas Shift Reaction over Pt-Based Catalysts. *J. Phys. Chem. C* **2016**, *120*, 10328−10339.
(111) Ammal, S. C.; Heyden, A. Water-Gas Shift Catalysis at Corner Atoms of Pt Clusters in Contact with a TiO2(110) Support Surface. *ACS Catal.* **2014**, *4*, 3654−3662.
(112) Walker, E. A.; Mitchell, D.; Terejanu, G. A.; Heyden, A. Identifying Active Sites of the Water-Gas Shift Reaction over Titania Supported Plantinum Catalysts under Uncertainty. *ACS Catal.* **2018**, *8*, 3990−3998.
(113) Greeley, J.; Mavrikakis, M. Competitive Paths for Methanol Decomposition on Pt(111). *J. Am. Chem. Soc.* **2004**, *126*, 3910−3919.
(114) Greeley, J.; Mavrikakis, M. A First-Principles Study of Methanol Decomposition on Pt(111). *J. Am. Chem. Soc.* **2002**, *124*, 7193−7201.
(115) Desai, S. K.; Neurock, M.; Kourtakis, K. A Periodic Density Functional Theory Study of the Dehydrogenation of Methanol over Pt(111). *J. Phys. Chem. B* **2002**, *106*, 2559−2568.
(116) García-Muelas, R.; Li, Q.; López, N. Density Functional Theory Comparison of Methanol Decomposition and Reverse Reactions on Metal Surfaces. *ACS Catal.* **2015**, *5*, 1027−1036.
(117) Zhou, C.; Wu, J.; Dhilip Kumar, T. J.; Balakrishnan, N.; Forrey, R. C.; Cheng, H. Growth Pathway of Pt Clusters on α-Al2O3(0001) Surface. *J. Phys. Chem. C* **2007**, *111*, 13786−13793.
(118) Zandkarimi, B.; Alexandrova, A. N. Dynamics of Subnanometer Pt Clusters Can Break the Scaling Relationships in Catalysis. *J. Phys. Chem. Lett.* **2019**, *10*, 460−467.
(119) Nigam, S.; Majumder, C. Orr Viability of Alumina-Supported Platinum Nanocluster: Exploring Oxidation Behavior by DFT. *Phys. Chem. Chem. Phys.* **2017**, *19*, 19308−19315.
(120) Shi, X.-R.; Sholl, D. S. Nucleation of Rhn (n = 1-5) Clusters on γ-Al2O3 Surfaces: A Density Functional Theory Study. *J. Phys. Chem. C* **2012**, *116*, 10623−10631.
(121) Mehmood, F.; Greeley, J.; Curtiss, L. A. Density Functional Studies of Methanol Decomposition on Subnanometer Pd Clusters. *J. Phys. Chem. C* **2009**, *113*, 21789−21796.

(122) Singh, R.; Biswas, P.; Jha, P. K. Density Functional Theory Investigation of Structure, Stability, and Glycerol/Hydrogen Adsorption on Cu, Cu-Zn, and Cu-Zno Clusters. *Quantum Chem.* **2020**, *120*, No. e26239.
(123) Ammal, S. C.; Heyden, A. Nature of Ptn/TiO2(110) Interface under Water-Gas Shift Reacton Conditions: A Constrained Ab Initio Thermodynamics Study. *J. Phys. Chem. C* **2011**, *115*, 19246−19259.
(124) Copeland, J. R.; Foo, G. S.; Harrison, L. A.; Sievers, C. In Situ ATR-IR Study on Aqueous Phase Reforming Reactions of Glycerol over a Pt/γ-Al2O3 Catalyst. *Catal. Today* **2013**, *205*, 49−59.
(125) Réocreux, R.; Girel, É.; Clabaut, P.; Tuel, A.; Besson, M.; Chaumonnot, A.; Cabiac, A.; Sautet, P.; Michel, C. Reactivity of Shape-Controlled Crystals and Metadynamics Simulations Locate the Weak Spots of Alumina in Water. *Nat. Commun.* **2019**, *10*, No. 3139.
(126) Fang, Z.; Wang, Y.; Dixon, D. A. Computational Study of Ethanol Conversion on Al8O12 as a Model for γ-Al2O3. *J. Phys. Chem. C* **2015**, *119*, 23413−23421.
(127) Christiansen, M. A.; Mpourmpakis, G.; Vlachos, D. G. Density Functional Theory-Computed Mechanisms of Ethylene and Diethyl Ether Formation from Ethanol on γ-Al2O3(100). *ACS Catal.* **2013**, *3*, 1965−1975.
(128) Hine, N. D. M.; Frensch, K.; Foulkes, W. M. C.; Finnis, M. W. Supercell Size Scaling of Density Functional Theory Formation Energies of Charged Defects. *Phys. Rev. B* **2009**, *79*, No. 024112.
(129) Sorescu, D. C.; Boatz, J. A.; Thompson, D. L. First-Principles Calculations of the Adsorption of Nitromethane and 1,1-Diamino-2,2-Dinitroethylene (Fox-7) Molecules on the Alpha-Al2O3(0001) Surface. *J. Phys. Chem. B* **2005**, *109*, 1451−1463.
(130) Sun, G.; Alexandrova, A. N.; Sautet, P. Pt8 Cluster on Alumina under a Pressure of Hydrogen: Support-Depedent Reconstructino from First-Principles Global Optimization. *J. Chem. Phys.* **2019**, *151*, No. 194703.
(131) Kresse, G.; Furthmuller, J. Efficient Iterative Schemes for Ab Initio Total-Energy Calculations Using a Plane-Wave Basis Set. *Phys. Rev. B* **1996**, *54*, 11169−11186.
(132) Kresse, G.; Hafner, J. Ab Initio Molecular Dynamics for Liquid Metals. *Phys. Rev. B* **1993**, *47*, 558−561.
(133) Kresse, G.; Hafner, J. Ab Initio Molecular-Dynamics Simulation of the Liquid-Metal-Amorphous-Semiconductor Transition in Germanium. *Phys. Rev. B* **1994**, *49*, 14251−14269.
(134) Perdew, J. P.; Burke, K.; Ernzerhof, M. Generalized Gradient Approximation Made Simple. *Phys. Rev. Lett.* **1996**, *77*, 3865−3868.
(135) Perdew, J. P.; Burke, K.; Ernzerhof, M. Erratum: Generalized Gradient Approximation Made Simple. *Phys. Rev. Lett.* **1997**, *78*, 1396.
(136) Kresse, G.; Joubert, D. From Ultrasoft Pseudopotentials to the Projector Augmented-Wave Method. *Phys. Rev. B* **1999**, *59*, 1758−1775.
(137) Grimme, S.; Antony, J.; Ehrlich, S.; Krieg, H. A Consistent and Accurate Ab Initio Parameterization of Density Functional Dispersion Correction (DFT-D) for the 94 Elements H-Pu. *J. Chem. Phys.* **2010**, *132*, No. 154104.
(138) Grimme, S.; Ehrlich, S.; Goerigk, L. Effect of the Damping Function in Dispersion Corrected Density Functional Theory. *J. Comput. Chem.* **2011**, *32*, 1456−1465.
(139) Monkhorst, H. J.; Pack, J. D. Special Points for Brillouin-Zone Integrations. *Phys. Rev. B* **1976**, *13*, 5188−5192.
(140) Bodenschatz, C. J.; Xie, T.; Zhang, X.; Getman, R. B. Insights into How the Aqueous Environment Influences the Kinetics and Mechanisms of Heterogeneously-Catalyzed COH* and CH3OH* Dehydrogenation Reactions on Pt(111). *Phys. Chem. Chem. Phys.* **2019**, *21*, 9895−9904.
(141) Zhu, J.; Getman, R. B. Reaction Pathways and Microkinetic Modeling of n-Butane Oxidation to 1-Butanol on Cu, Cu3Pd, Pd, Ag3Pd, and PdZn (111) Surfaces. *Ind. Eng. Chem. Res.* **2018**, *57*, 5580−5590.
(142) Henkelman, G.; Jonsson, H.; Uberuaga, B. P. A Climbing Image Nudged Elastic Band Method for Finding Saddle Points and Minimum Energy Paths. *J. Chem. Phys.* **2000**, *113*, 9901−9904.
(143) Henkelman, G.; Jonsson, H. Improved Tangent Estimate in the Nudged Elastic Band Method for Finding Minimum Energy Paths and Saddle Points. *J. Chem. Phys.* **2000**, *113*, 9978−9985.
(144) Henkelman, G.; Jonsson, H. A Dimer Method for Finding Saddle Points on High Dimensional Potential Surfaces Using Only First Derivatives. *J. Chem. Phys.* **1999**, *111*, 7010−7022.
(145) Dix, S. T.; Gómez-Gualdrón, D. A.; Getman, R. B. Implications of Sterically Constrained n-Butane Oxidation Reaction Pathways over Ag3Pd(111) on the Design of MOF-Encapsulated Catalysts. *Surf. Sci.* **2016**, *653*, 11−21.
(146) Ravenelle, R. M.; Copeland, J. R.; Van Pelt, A. H.; Crittenden, J. C.; Sievers, C. Stability of Pt/γ-Al2O3 Catalysts in Biomass Solutions. *Top. Catal.* **2012**, *55*, 162−174.
(147) Copeland, J. R.; Shi, X.-R.; Sholl, D. S.; Sievers, C. Surface Interactions of C2 and C3 Polyols with γ-Al2O3 and the Role of Coadsorbed Water. *Langmuir* **2013**, *29*, 581−593.
(148) So, J.; Chung, Y.; Sholl, D. S.; Sievers, C. In-Situ ATR-IR Study of Surface Reaction During Aqueous Phase Reforming of Glycerol, Sorbitol and Glucose over Pt/γ-Al2O3. *Mol. Catal.* **2019**, *475*, No. 110423.
(149) Zhang, X.; Sewell, T. E.; Glatz, B. N.; Sarupria, S.; Getman, R. B. On the Water Structure at Hydrophobic Interfaces and the Roles of Water on Transition-Metal Catalyzed Reactions: A Short Review. *Catal. Today* **2017**, *285*, 57−64.
(150) Bodenschatz, C. J.; Sarupria, S.; Getman, R. B. Molecular-Level Details About Liquid H2O Interactions with CO and Sugar Alcohol Adsorbates on Pt(111) Calculated Using Density Functional Theory and Molecular Dynamics. *J. Phys. Chem. C* **2015**, *119*, 13642−13651.

https://dx.doi.org/10.1021/acs.jpcc.0c03717
J. Phys. Chem. C 2020, 124, 19015−19023